applied sciences

MDPI

Article

A Study on Stress Evolution Patterns and Energy Fields in High-Seam-Height Working Faces in Folded Structures

Fukun Xiao [1,*], Zongchao Qu [2,3], Pan Wu [4] and Qingshou Hou [1]

[1] School of Mining Engineering, Heilongjiang University of Science and Technology, Harbin 150022, China
[2] School of Safety Engineering, Heilongjiang University of Science and Technology, Harbin 150022, China
[3] National Mine Safety Administration, Heilongjiang Bureau, Harbin 150022, China
[4] Cuncaota Coal Mine, Guoneng Shendong Coal Group Co., Ltd., Ordos 017209, China
* Correspondence: xiaofukun@hotmail.com

Abstract

To address the alternating high- and low-stress cycles observed during the analysis of stress evolution and energy field distribution in the folded structural zone of Working Face No. 2 at a certain mine, a three-dimensional geological numerical model was established using Rhino+HyperMesh, incorporating the geological characteristics of the working face. Additionally, a dual-yield model for the goaf was incorporated into the analysis to accurately capture rock behavior. The analysis reveals that in the folded structural zone, the stress at the advance supports reaches its maximum at each inflection point, when the waste rock in the goaf also exhibits significant hardening behavior. Specifically, during the synclinal upward mining stage, the abutment stress reaches 7.6 MPa. In contrast, stress values reach their minimum at the ridge and trough points. In these inflection points, concentrated stresses are also observed on both sides of the coal face in the goaf. Notably, the stress in the haulage gate, due to its greater curvature, is higher than that in the return air drift. Furthermore, the strain energy peaks at the hinge point between the drift and the axis of the anticline. This concentration of strain energy occurs in areas highly prone to roof collapse, and notably, it is maximized where these three factors intersect.

Keywords: fold structure; Flac3D; abutment stress; strain energy

1. Introduction

As one of the most widespread geological structures, the formation and evolution of the stress field in fold structures have attracted significant attention from scholars due to their impact on coal mining [1–3]. Compared to horizontal coal and rock strata, the stress distribution in mining areas is uneven due to the effects of fold structures, with horizontal stress being the dominant component. High horizontal stress is typically concentrated in the synclinal axis [4,5] and the axial zone of the anticline [6,7]. Under the disturbance caused by mining operations, energy accumulates in the roof, thereby inducing rockburst disasters [8,9], which pose a serious threat to the safety of workers and significantly impact daily production.

Currently, scholars have conducted extensive research on stress distribution in folded structures. Ju Xin [10] derived a formula for calculating rock mass pressure in folded structures, elucidating the pattern by which structural stress transitions from tensile to compressive stress with increasing burial depth, thereby providing a stress field basis for rockburst hazard assessment [11]. Wang Shengben et al. [12] established a fold model

Academic Editor: Ricardo Castedo Ruiz

Received: 12 April 2026
Revised: 6 May 2026
Accepted: 8 May 2026
Published: 12 May 2026

to systematically elucidate the evolution patterns of the displacement field and stress field in coal bodies. Cheng et al. [13] revealed the characteristics of non-uniform stress evolution and intensified stress concentration in working faces within fold structures, noting that stresses in the axial part of synclines are higher than in the flanks and are more likely to trigger high-energy microseismic events [14]. Kang Hongpu et al. [15,16] used field measurements and modeling to reveal the characteristics of the tectonic stress field, showing that the increase in horizontal stress in the axial part of the syncline is significantly greater than in the flanks. Tang Long et al. [17] pointed out that stress concentration is most pronounced at the crests of folded structures, and that the greater the curvature, the more non-uniform the stress distribution [18]. Studies by Guo et al. [19] and Bai et al. [20] indicate that stress is asymmetrically distributed in fault-fold composite structural zones, with higher stress along the synclinal axis; the superposition of tectonic and mining-induced stresses significantly increases the risk of rockbursts. Cao et al. [21] noted that stress in fold structural zones exhibits a zonal distribution, with horizontal stress playing a dominant role and controlling the stability of surrounding rock in different regions [22]. Wang et al. [23] employed microseismic monitoring, energy density cloud analysis, and seismic velocity tomography to investigate the mechanism of rock bursts in synclinal structural zones. Zhouye et al. [24] and Wang et al. [25] found that the inner arc of the fold axis is the region of maximum principal stress concentration, and the coupling of mining-induced and tectonic stresses determines the location and intensity of the stress concentration zone; Liu Chang et al. [26] found that a decrease in coal seam dip angle within a folded structural zone exacerbates stress concentration in the tunnel and forms L-shaped high-stress zones.

Although theoretical analysis and statistical analysis are common methods for assessing the likelihood of rock mass instability, the limited scale of models, the complex physical and mechanical properties of coal and rock, and the influence of the longwall mining process make large-scale parametric analysis difficult to achieve. In contrast, numerical methods offer significant advantages in studying the mechanical behavior of deep surrounding rock [27]. Hamdi P et al. [28] employed FLAC3D numerical simulations and in situ stress measurements to find that the in situ stress in the study area is significantly controlled by topography and tectonics, with the stress state varying systematically along the tunnel axis; the distribution of excavation damage zones showed high consistency with the simulation results. Zhang et al. [29] used FLAC3D modeling to simulate fault slip and stress changes during mining, revealing the mechanism by which fault activation triggers rock bursts and determining that the coupling influence range between mining operations and fault activation is 150 m. Wang et al. [30] simulated and analyzed the evolution characteristics of the stress field in a fold structure region during the mining process and investigated the rock pressure laws in different areas of the fold structure under mining influence. Chen et al. [31] used numerical simulation to study the stress distribution patterns during the formation of fold structures and the laws governing local stress field changes induced by mining operations.

In summary, although scholars both domestically and internationally have achieved significant results regarding stress distribution in folded structures, existing research still focuses on static mechanical responses under conventional mining heights. The intense overburden movement and extensive spatial disturbances triggered by deep-seam mining result in a synergistic evolution mechanism of the mining-induced stress field and energy field under fold constraints that differs significantly from traditional operating conditions. Furthermore, existing numerical models still lack sufficient consideration of the nonlinear bearing characteristics of waste rock in the goaf. Therefore, this paper takes a high-seam longwall face in the No. 2 coal seam of a certain mine as the engineering background. Using Rhino–Hypermesh, a detailed 3D geological model was constructed, and the Double-Yield

criterion was introduced to reproduce the bearing characteristics of the goaf [32]. The study investigates the evolution of the stress field and the distribution of energy in high-seam longwall faces across folded structural zones, providing theoretical support and scientific basis for the prevention and control of rock bursts in such complex structural zones.

2. Project Background

This paper takes the full-height fully mechanized mining face in the first mining cycle of Coal Seam No. 2 in a certain mining area as its project background. This face exhibits typical characteristics of mining-induced activation in a folded structure, is controlled solely by the folded structure, and has no pre-existing through faults or slip planes. The coal seam roof consists of a composite of sandy mudstone. The overlying bedrock layer ranges in thickness from 240 to 280 m, and the loose sedimentary layer ranges from 7 to 17 m in thickness. When the face advanced to a point 210 m behind the go-ahead, roof instability occurred in the control zone of hydraulic supports No. 105 to No. 125. The unstable zone extended 10.8 m along the strike and was 8.3 m from the solid coal face of the return airway. At this point, the tail end of the face conveyor had just passed through a structural depression, and the face was in an inclined mining state. Under concentrated structural stress, large-scale shear slippage occurred along the coal face. As the working face continued to advance, the unstable zone expanded to the area between supports No. 150 and No. 156, and the height of the roof collapse increased from an initial 3 m to 6–8 m in the later stages. The impact of the instability persisted for six working cycles, as shown in Figure 1.

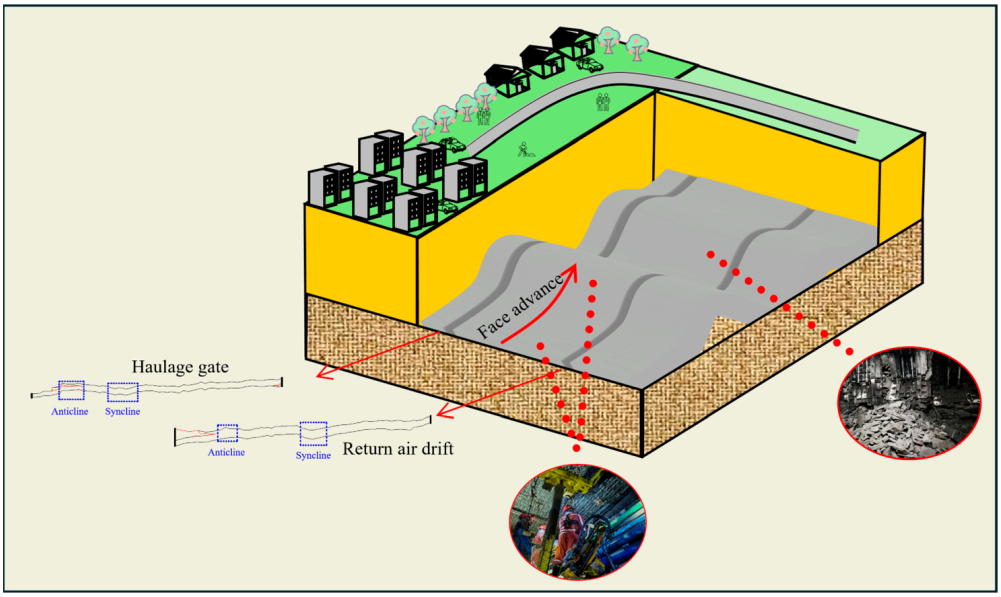

Figure 1. Overview of No. 2 Coal Seam Working Face.

Figure 2 integrates the weighting interval with topographic data and classifies the inflection points into eight distinct stages based on the coal seam stratigraphy; Stages 2 through 7 correspond to the six observed field cycles of instability evolution. Based on the support load analysis in Figure 2, the first pressure surge on the working face occurs during Stage 2. In Stage 2, the coal seam is located in an anticline structural zone, where the roof is subject to tensile structural stress and is prone to fracturing, making roof falls highly likely. Furthermore, both Stage 2 and Stage 8 involve nearly horizontal coal seams, and the periodic pressure surges in these mining cycles exhibit regularity. Compared with other stages, the differences in the intervals and durations of these periodic pressure surges are

relatively small. Stages 3 and 4 are in the down-dip mining area. At this stage, the working face experiences both large and small periodic pressure cycles, with varying cycle intervals and durations. Among these, the 6th cycle has the shortest interval and duration, at 3.6 m and 2.7 m, respectively. At this time, the working face is in the initial mining phase of the coal seam corner, and the immediate roof has not yet formed a stable arch-beam structure. In Stage 5, the face advanced in an upward, inclined mining direction. Under the influence of horizontal tectonic compressive stress, the periodic pressure wave spacing was relatively large. The 12th periodic pressure wave occurred at an advanced distance of 206 m, with a spacing of 22 m, which was the maximum value during this mining cycle.

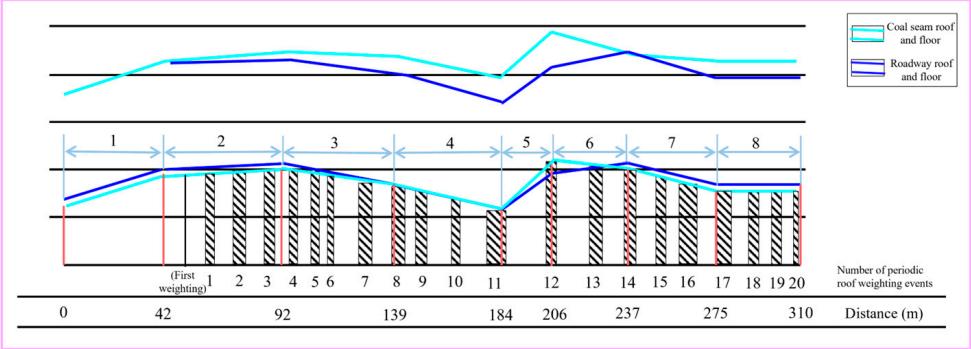

Figure 2. Map of incoming pressure in folded terrain.

3. Analysis of Stress Evolution Characteristics in the Working Surface of the Folded Structure Zone

3.1. Development of Numerical Model

To systematically elucidate the spatiotemporal evolution of the mining-induced stress field in a folded structural zone, a three-dimensional overburden structural model incorporating the folded structure was established, using the high-seam longwall face in Coal Seam No. 2 as a case study. This study establishes a numerical model based on changes in surrounding rock stress during the advance of the working face across the irregular topography of the fold. The fold is treated as a continuous curved rock mass for simulation analysis, and the model is constructed using the Rhino–Hypermesh finite element method. The actual geological numerical model of the fold structure zone is shown in Figure 3. The model dimensions are 500 m × 300 m × 200 m, with a total of 1,268,458 model elements. The Mohr–Coulomb constitutive model was adopted, whilst a dual-yield constitutive model was selected for the goaf to characterize the stress–strain mechanical properties of the goaf waste rock's strain hardening. The fundamental physical and mechanical parameters of the coal and rock were derived from rock block mechanical tests conducted at the mine. It should be noted that rock masses in actual fold-structured zones often exhibit high variability and anisotropy. Due to the computational constraints of large-scale modeling, the model employs the continuous medium approach to simplify the rock mass as an isotropic medium. Inter-layer contacts, rock mass fracturing and weak-plane shear effects have been accounted for through the reduction and generalization of rock mechanical parameters based on the Hoek–Brown criterion, thereby providing a macroscopic representation of the stress and energy evolution patterns in the surrounding rock of the fold zone. The physical and mechanical parameters of the coal and rock mass are shown in Table 1.

Table 1. Mechanical Parameters of Coal Rock Body.

Lithology	Bulk Modulus (GPa)	Shear Modulus (GPa)	Cohesion (MPa)	Angle of Internal Friction (°)	Tensile Strength (MPa)	Density (kg/m^3)
Medium-grained sandstone	5.5	2.9	3.75	32	2.42	2490
Fine sandstone	7.02	3.6	4.8	31	2.45	2560
Coarse-grained sandstone	4.4	2.04	3.15	33	2.42	2410
Siltstone	7.62	4.1	2.98	35	3.54	2650
Coal	1.73	0.89	1.5	25	0.46	1750

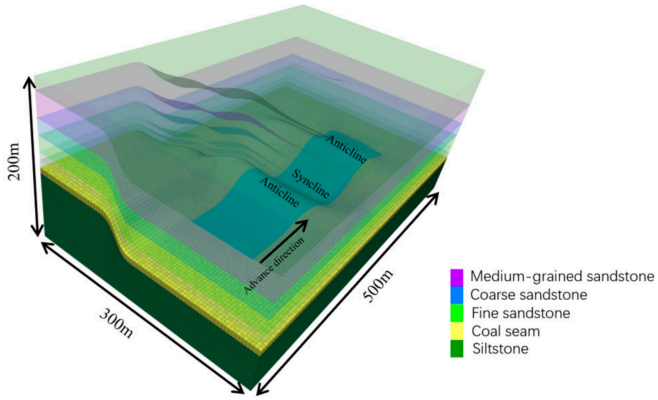

Figure 3. Actual Geological Numerical Model of Fold Tectonic Zone.

This numerical model employs a multi-level composite boundary condition system to implement mechanical constraints on the geological prototype. The model boundary conditions are set according to the following guidelines: full-degree-of-freedom constraints are applied to the front, rear, and bottom surfaces of the model, and displacement boundary control was achieved using the zero-velocity method. Based on the burial depth of 112 m at Working Face No. 2, a vertical stress of 3.75 MPa is applied to simulate the overburden stress field. The lateral pressure coefficient is set to 1.5. Stress-loading boundary conditions are applied to the left and right boundaries, where a distributed loading system is established to construct a depth-dependent structural stress gradient field, with the horizontal stress components satisfying the lateral pressure coefficient. The model employs the continuous medium method. Interlayer contacts, rock mass fracturing, and shear effects at weak planes are generalized using rock mechanical parameters, enabling a macroscopic representation of stress and energy evolution in the surrounding rock of the fold zone. The numerical model maintains in situ stress equilibrium prior to mining disturbance, converging to the residual stress norm through iterative calculations to achieve initial stress equilibrium. The specific workflow in the numerical simulation is as follows: During model initialization, the composite stress field is constructed using the Initial command. The gravitational stress field is implemented using the Set gravity command to apply a gravitational acceleration of 9.8 m/s^2. The tectonic stress field is modeled using the Gradient keyword to represent the nonlinear distribution of horizontal stress with depth. Additionally, a stepwise loading strategy is employed to achieve mechanical equilibrium of the geological prototype: first, the model is set to an elastic constitutive model for elastic pre-equilibrium; subsequently, a Mohr–Coulomb constitutive model is applied to gradually approximate the true stress state; finally, a rock stress distribution consistent with engineering reality is obtained, as shown in Figure 4. It is worth noting that to eliminate the influence of deformations that may occur during the initial equilibrium process on subsequent coal seam mining, a displacement field reset operation must be performed after completing the initial equilibrium. This enables an accurate analysis of the model's force and deformation characteristics under disturbances caused by coal seam mining.

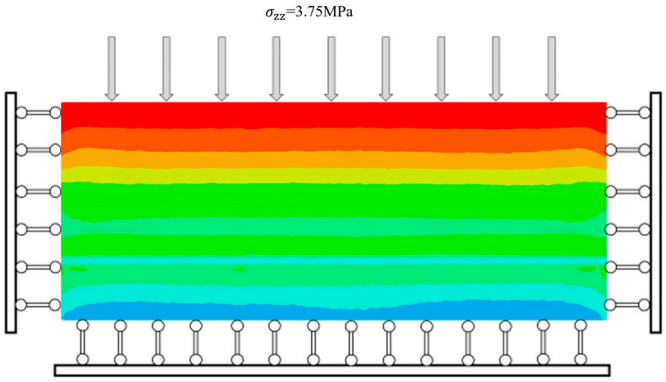

(**a**) Self-weight stress field and boundary loads

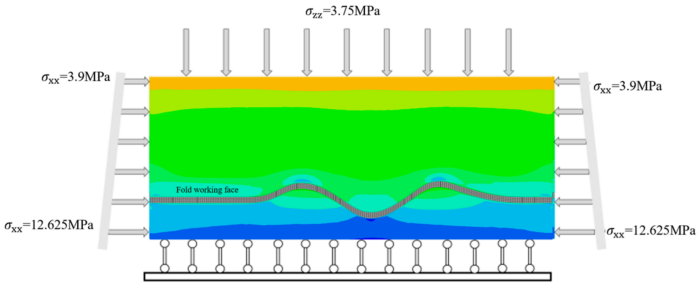

(**b**) Stress field and boundary loads in a folded structure

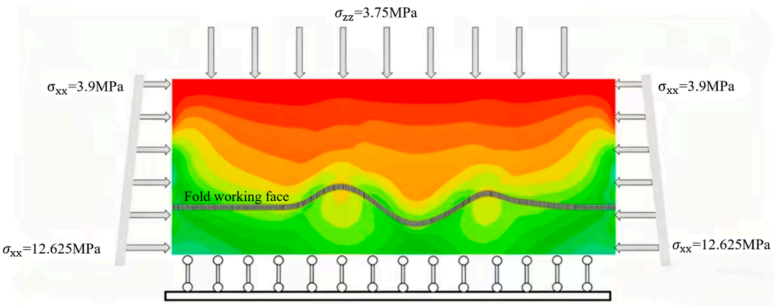

(**c**) Vertical stress field and boundary loads in a corrugated structure

Figure 4. Initial stress field and boundary conditions of the model.

As shown in Figure 4, the initial stress field of the source rock indicates that fold structures alter the magnitude of horizontal stress at the same elevation. The degree of horizontal stress concentration in the axial zones of synclines and anticlines is higher than in other areas at the same elevation. Furthermore, under the influence of tectonic stress, the degree of horizontal stress concentration in the axial zone of an anticline—which is shallower and has greater curvature—is actually greater than that in the axial zone of an anticline that is deeper and has smaller curvature. It follows that the axial zones of folds, as characteristic points, are critical areas requiring special attention during the advancement of mining faces.

3.2. The Evolution of Abutment Stress Along the Strike of the Working Face in the Folded Structure Zone

Inflection points and troughs in folded structures often create zones of abnormal stress concentration. These zones pose a significant threat to the stability of the surrounding rock system in mining areas [17]. By establishing a dynamic stress field model for regions affected by fold structures and focusing on stress distribution and evolution at key locations, it becomes possible to understand the spatiotemporal evolution of the surrounding rock

stress field during mining operations. This knowledge provides theoretical support for formulating targeted measures to control the surrounding rock.

As shown in Figure 5a, when the working face enters the upward mining phase of an anticline following horizontal mining, it passes through a zone of reduced in situ stress. The stress gradient of the advance support decreases once the advance abutment stress has reached its maximum value of 5.75 MPa. As the working face advances, it reaches a minimum value of 4.84 MPa at the anticline crest and, Behind the working face, the roof of the goaf broke and subsided at the turning end of the fold. After lagging behind the working face by a certain distance, the waste rock begins to effectively support the roof, generating a support force of approximately 1 MPa. This waste rock support force reaches a maximum of 1.53 MPa at the inflection point. The direct roof above the mined area is prone to failure after mining; the underlying primary roof subsequently bends and subsides, coming into contact with the waste rock to re-form a stress concentration zone. The waste rock, after being continuously compressed, exerts a reaction force on the roof and, together with the coal wall of the goaf and the hydraulic supports, jointly supports the roof until stability is achieved.

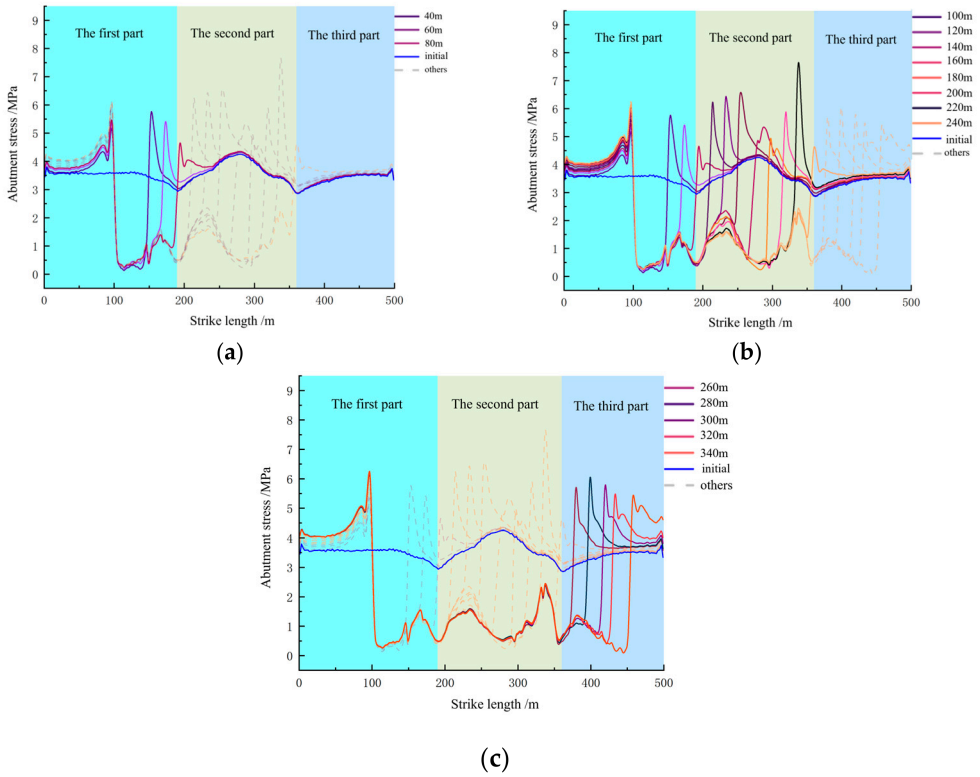

Figure 5. Abutment stress distribution curve of working face at different propulsion distances. (**a**) Up-dip mining stage of the working face on an anticline. (**b**) Transition stage of the working face across an anticline into a syncline. (**c**) Down-dip mining stage of the working face on an anticline.

As shown in Figure 5b, as the working face advances toward the back-anticline transition zone, mining-induced dynamic disturbances disrupt the original static tectonic stress equilibrium, causing stress to re-accumulate within the fold structures and energy to build up rapidly, thereby forming an activated tectonic stress zone. Static tectonic stress serves as the background field, while mining-induced unloading and stress transfer are the direct triggers for activation. The coupling of these two factors controls the evolution of stress in the surrounding rock of the working face, with mining-induced stress and tectonic stress jointly forming an irregular and complex stress field. In the initial cutting zone of the working face, the abutment stress on the coal face reaches a maximum level of 5.9 MPa;

under the influence of the activated tectonic stress field, the stress distribution exhibits a gradient-like increase from the anticline apex to the syncline trough, with both the bearing stress of the goaf waste rock and the surrounding rock stress of the working face displaying significant asymmetry along the structural strike, and stress concentration occurring at the inflection point. When the fully mechanized mining face approaches the structural zone at the synclinal trough point, the concentrated stress field ahead of the face undergoes significant release. This phenomenon reveals the regulatory mechanism by which the geometric morphology of fold structures influences the redistribution of mining-induced stress fields. When the working face advanced to 160 m, roof failure caused the abutment stress to begin decreasing; subsequently, the abutment stress at the infill zone inflection point increased. As the working face continued to advance, the degree of stress relief in the infill zone increased, reaching nearly 0 MPa at the fold trough point. When the working face advanced to 220 m from the cut-off point, the advance abutment stress in the folded CMM working face reached a peak of approximately 7.6 MPa. As the advance continued toward the ridge point, the roof fractured, and the abutment stress began to decrease. The measured point of roof instability (210 m) and the point of maximum incoming pressure (206 m) show a high degree of spatial correspondence with the simulated stress and energy peak point (220 m), with a positional deviation of only approximately 4.7% to 6.7%, which falls within the permissible error range for numerical simulation. The model is capable of accurately reproducing the stress evolution characteristics during the mining process of deep-seam longwall faces in folded structural zones.

Figure 5c: When the working face enters the down-dip mining stage of the anticline, the surrounding rock is in a zone of elevated in situ stress. As the working face advances, the advance abutment stress gradually increases, reaching a peak vertical stress of 6.1 MPa at a distance of 280 m from the cut-off point. which also marks the inflection point of the anticline. As the face advances past the inflection point, the roof fractures and the abutment stress begin to decrease; at a distance of 300 m from the cut-off point, the peak vertical stress is 5.6 MPa, a 5% decrease. The bearing stress in the goaf increases continuously at the goaf inflection point. Consequently, the further the goaf lags behind the working face, the more pronounced the abutment capacity of the goaf waste becomes. This is because, after coal seam mining, it takes a certain amount of time for the waste rock to completely fill the goaf; therefore, the contact between the overlying strata and the waste rock often lags behind the working face by a certain distance.

3.3. The Evolution of Abutment Stress in the Surrounding Rock of Working Faces in Folded Structures

When the working face advances into different zones of a fold structure, the stress distribution in the advance support within the fold structure zone exhibits distinct regional characteristics. In terms of strike, when the working face advances to the vicinity of troughs and ridges within the fold structure zone, the abutment stress drops sharply, and the roof becomes extremely unstable. At the inflection points, the concentration of advance abutment stress is relatively high, and the waste rock in the goaf also exerts a significant supporting capacity on the primary roof at these points. This demonstrates that the characteristics of the fold structure have a significant impact on the stress distribution in the surrounding rock of the mining area.

During the development of roadways and the advancement of the mining face, differences in the distribution characteristics of in situ stress among various fold structure units result in spatial heterogeneity in mining production risks. When the fully mechanized mining face advances into zones with different mechanical properties within the fold structure, the stability of the surrounding rock exhibits significant variations. Therefore, the entire mining face advancement process is divided into three sections.

As shown in Figure 6, the working face is currently in the first stage of mining. The anticline structure is located in a stress reduction zone, while the goaf and the side roadways are experiencing excavation-induced stress relief, i.e., they are stress release zones. At this point, the working face is in the upward mining phase of the anticline. When the advance reaches 40 m, the working face is at a turning point, where advance stress concentration occurs in the roof. Due to changes in the coal seam dip angle, the pressure from the inclined roof above the coal face shifts forward, causing stress release in the roof of the goaf and resulting in stress concentration at the coal face of the working face. When the working face advances further to 60 m, it reaches the inflection point. The advance abutment stress in the roof decreases slightly, and stress concentration occurs in the crosscuts on both sides of the goaf. The abutment stress in the haulage crosscut is 5.82 MPa, while the return air drift abutment stress is 4.95 MPa. Analysis of single-fold structures indicates that the greater the curvature of the fold, the larger the difference between the additional stress caused by rock bending deformation and the principal stress. According to the Mohr–Coulomb yield criterion, the surrounding rock is more prone to stress accumulation [17]; therefore, the degree of stress concentration at the inflection point is also higher. When the working face advances to 80 m, it reaches the anticline crest, at which point the working face is located in a stress relief zone, and the advance abutment stress at the working face decreases significantly. Additionally, changes in the coal seam dip cause the immediate roof to fracture, resulting in roof collapse that propagates toward the goaf. Mining-induced fractures and fissures block the forward transmission of stress, causing it to develop along the side drifts on both sides of the goaf. The abutment stress in the haulage gate is 6.88 MPa, and in the return air drift, it is 5.71 MPa. When the roof near the headings reaches its strength limit, short-span fractures will form. Therefore, during the first stage of mining, the bearing stress in the headings on both sides of the goaf exhibits an increasing trend.

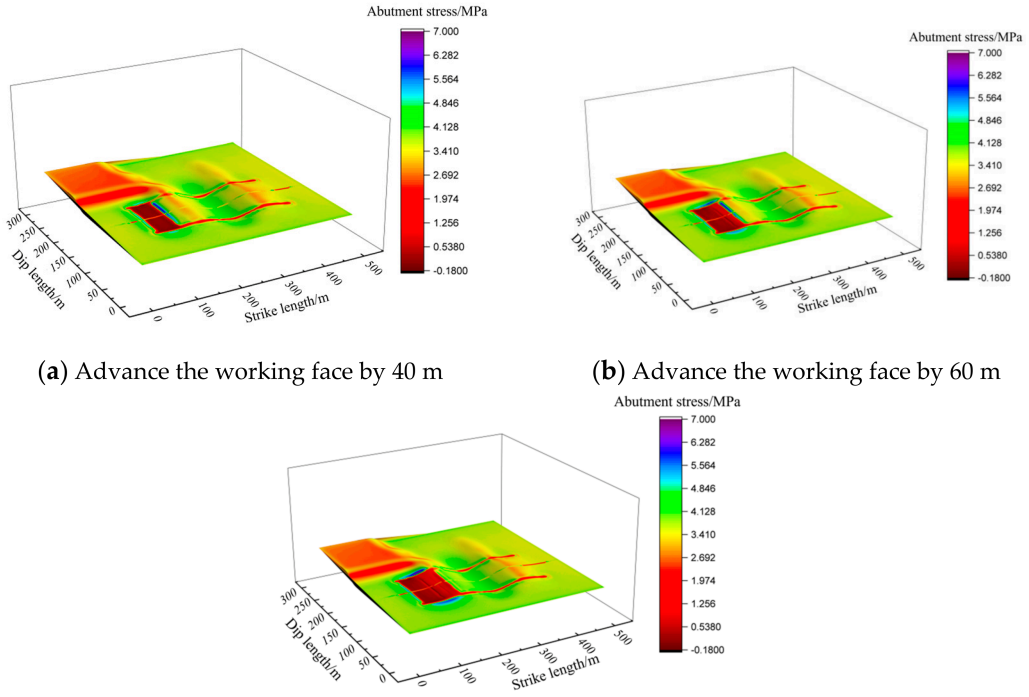

(**a**) Advance the working face by 40 m

(**b**) Advance the working face by 60 m

(**c**) Advance the working face by 80 m

Figure 6. A stress map of the surrounding rock in the first stage of the folded working face.

As shown in Figure 7, when the working face advances into the synclinal fold zone, the initial phase involves downward mining along the syncline. After the working face

passes the anticline crest, it re-enters the stress concentration zone and proceeds with downward mining. The stress concentration zone primarily encompasses the area ahead of the working face and the regions on both sides of it. When the working face advances to 100 m, the surrounding rock stress does not exhibit regional characteristics, and the roof of the working face remains relatively stable. At the inflection point of the first stage, the abutment stresses on both sides of the drift also begin to drop sharply, to 4.92 MPa and 4.34 MPa. When the working face advances to 120 m, viewed from the direction of advance, it reaches the anticline's inflection point. At this point, a stress concentration is observed in the advanced support. Viewed along the length of the working face, the roof in the inflection point region exhibits stress concentration in the advance support and displays a zonal effect, with the abutment stress on the return air drift side being significantly greater than that on the haulage gate side—completely opposite to the stress distribution in the first stage. When the working face advances to 140 m, it passes through the inflection point and remains within the stress concentration zone. The advance abutment stress exhibits the same zonal phenomenon, but the abutment stress in the haulage gate—located in the region of strong structural stress—is greater than that in the return air drift, at 6.91 MPa and 4.93 MPa, respectively, following the pattern that stress concentration is higher on the side of the fold structure with greater curvature. When the working face advances to 200 m, it enters the synclinal inflection point zone. At this point, stress concentration is greater at the inflection points of both side drifts, with abutment stresses of 7.24 MPa and 6.22 MPa. Conversely, the advanced abutment stress at the working face drops sharply, reaching a trough value. Analysis suggests that long-span roof cracks may develop here, or even roof failure, with the advance abutment stress shifting toward both sides of the goaf.

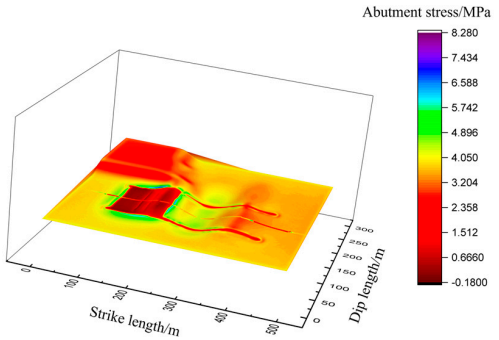

(**a**) Advance the working face by 100 m

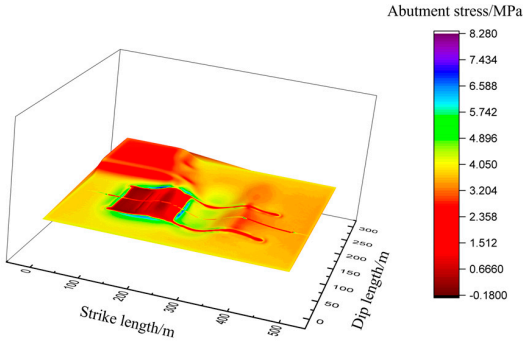

(**b**) Advance the working face by 120 m

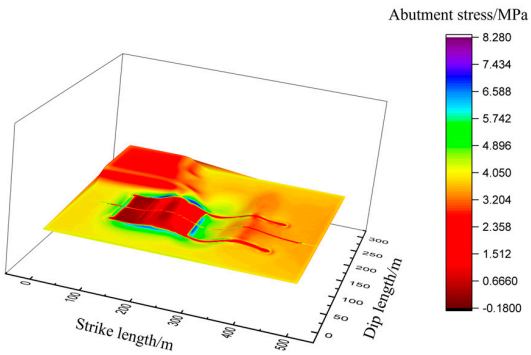

(**c**) Advance the working face by 140 m

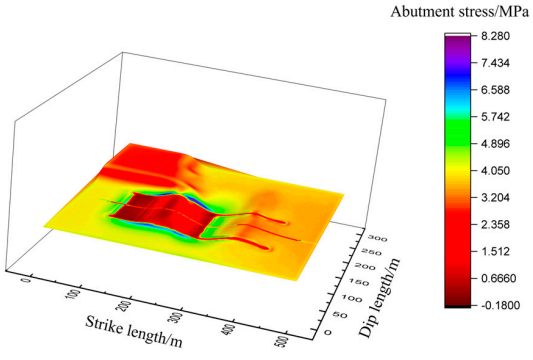

(**d**) Advance the working face by 160 m

(**A**) Surrounding rock stress map—down-dip mining on an anticline.

Figure 7. *Cont.*

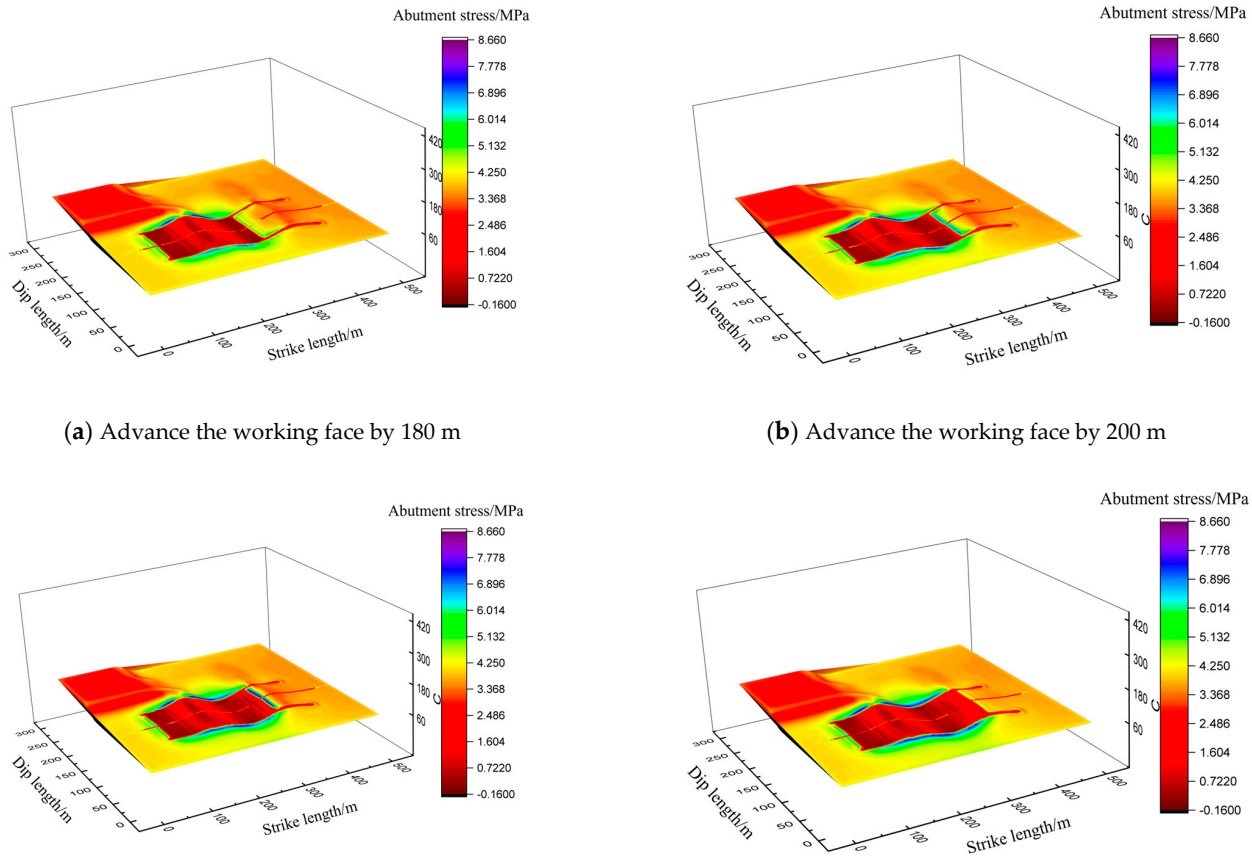

(**a**) Advance the working face by 180 m

(**b**) Advance the working face by 200 m

(**c**) Advance the working face by 220 m

(**d**) Advance the working face by 240 m

(**B**) Surrounding rock stress map—up-dip mining on a syncline.

Figure 7. Stress distribution in surrounding rock at second-stage folding working face.

After the working face passes through the synclinal trough point, the synclinal upward mining phase begins. When the working face advances to 180 m, the overhang distance of the goaf roof is short, the advance abutment stress at the working face is low, and stress reduction is observed in both side drifts deep within the goaf. When the working face advances to 200 m, the advance abutment stress begins to increase. Since the curvature of the folds is consistent along the length of the working face—indicating a single fold structure—no regional variations in abutment stress are observed. When the working face advances to 220 m, it reaches the third inflection point region, where the advance abutment stress reaches its peak value of 7.64 MPa, and the stress distribution is uniform; As the working face continues to advance to 240 m, it reaches the anticline crest. At this point, the working face is in the stress release zone, where the advance abutment stress decreases significantly. Furthermore, changes in the coal seam dip cause immediate roof fractures, leading to roof collapse that propagates toward the goaf. Mining-induced fractures and fissures block the forward transmission of stress, causing it to develop along the side drifts on both sides of the goaf. At this point, the abutment stress in the haulage gate increased to 7.23 MPa, and that in the return air drift reached 7.12 MPa. Once the roof near the drifts reaches its strength limit, short-span cracks will form; once these cracks propagate, the roof ultimately undergoes "O-X" fracturing.

As shown in Figure 8, the working face in the folded structure zone advanced through the anticline crest to the third stage, at which point the working face began down-dip mining. When the working face reached 180 m, the curvature of the folds was relatively small, at this point, mining is nearly horizontal, so the stress from the fold structure is

relatively low, and the abutment stress is primarily concentrated in the synclinal structural zone, while the advance abutment stress at the working face is relatively low. When the working face advances to 200–220 m, it passes through the fourth inflection point of the fold structure zone, and the abutment stress begins to increase. As the advance continues and the working face passes the turning point, the abutment stress begins to decrease again. Throughout this stage, strong abutment stress is observed in the drift on both sides of the goaf in the synclinal structure zone.

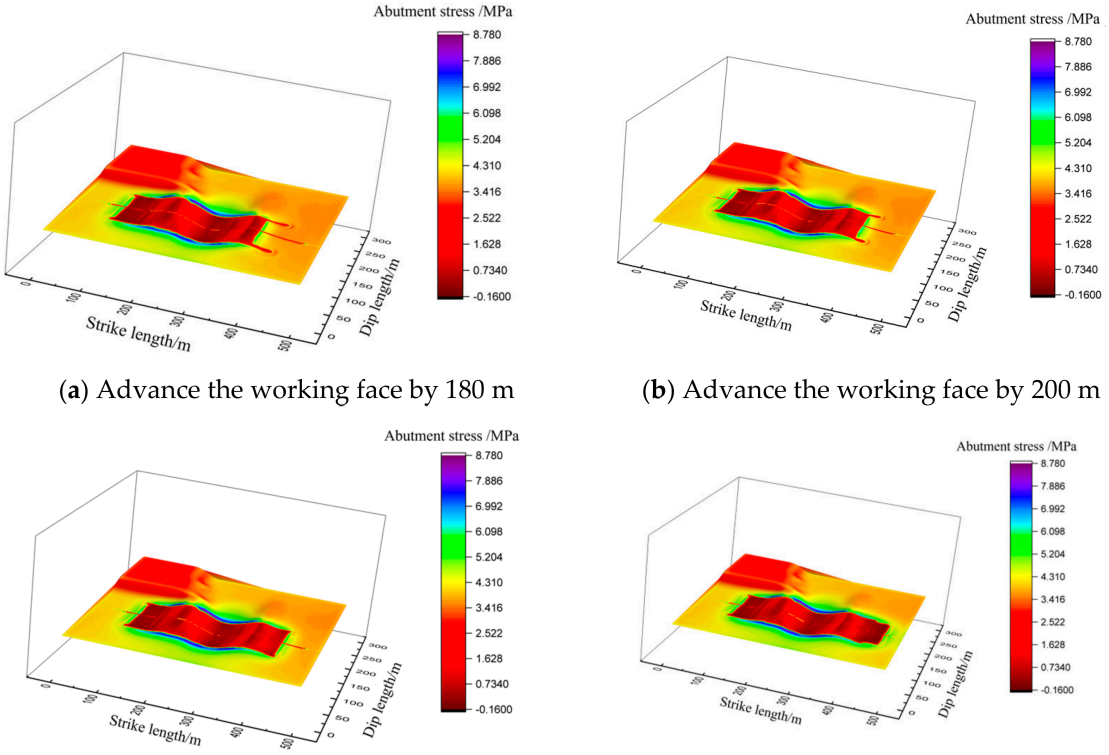

(**a**) Advance the working face by 180 m (**b**) Advance the working face by 200 m

(**c**) Advance the working face by 220 m (**d**) Advance the working face by 240 m

Figure 8. A stress map of the surrounding rock in the third stage of the folded working face.

Figure 9 shows the variation in stress in the surrounding rock of the working face at different advance distances. As shown in the figure, throughout the entire mining process, stress concentration occurs in the surrounding rock of the working face due to mining-induced disturbances. Stress concentrations are primarily located at the leading coal face of the working face and on both sides of the goaf, while the roof and floor of the working face are regions of reduced stress. In the dip direction, due to differences in curvature within the folded structural zone, the curvature is greater on the side adjacent to the haulage gate. Consequently, the abutment stress on the coal face wall on the goaf side is higher than that on the return air drift side. Furthermore, the distribution of high-stress zones near the drifts is highly consistent with the distribution of inflection points in the folded working face. It is worth noting that, due to the upward-dipping mining in the working face shown in Figure 9a,c, the gradient of change in advance abutment stress is greater, and the degree of stress concentration at the inflection point is higher. Furthermore, the gravitational component generated by the coal seam dip increases along the dip direction. Under these conditions, the coal seam roof is prone to failure and instability, particularly near the haulage gate, where roof stability is poorer and more likely to trigger roof falls.

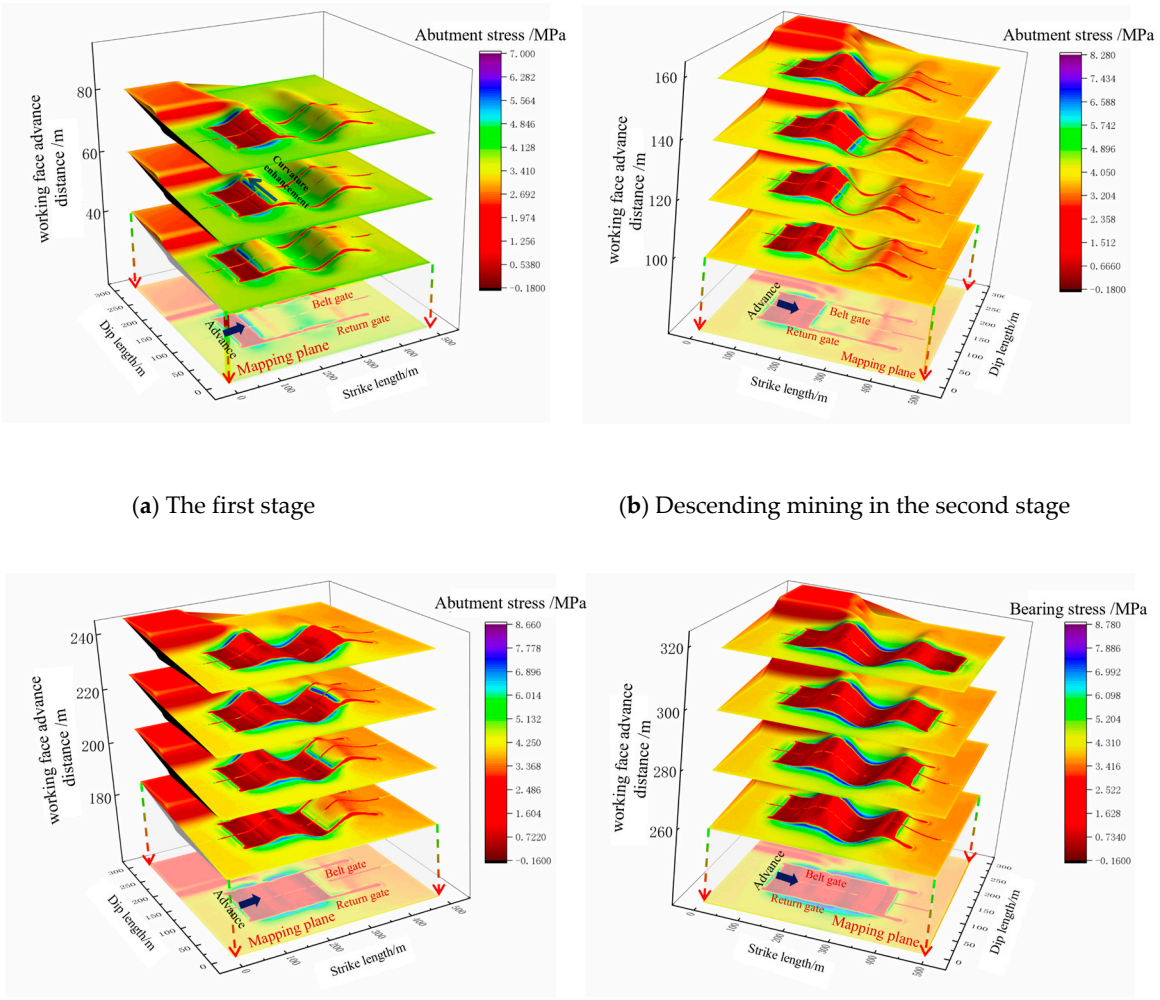

(**a**) The first stage

(**b**) Descending mining in the second stage

(**c**) Ascending mining in the second stage

(**d**) The third stage

Figure 9. Contour plot of abutment stress distribution at different advance distances in No. 2 coal seam working face.

4. Energy Field Distribution at the Working Surface of the Folded Structure Zone

Under complex stress conditions in the surrounding rock, studying the evolution of abutment stress alone is insufficient to explain the plastic failure and rupture of a working face. Energy serves as the intrinsic driving force behind roof failure; therefore, the stability of the roof in folded working faces will be analyzed from an energy perspective below.

4.1. Analytical Expression for the Second Invariance of Partial Stresses

Energy changes occur throughout the entire process of coal-rock mass deformation. Under the influence of mining-induced stresses, elastic energy can accumulate and be released. When the elastic energy stored in the coal rock mass reaches a critical value, it is converted into other forms of energy, leading to global failure and instability. Elastic energy primarily consists of strain energy and volumetric energy. Under external forces, the deformation of a material can be decomposed into two types: volumetric deformation and shape deformation. According to plasticity theory, volume changes are elastic; during plastic deformation, the volumetric strain of an object is zero or the average positive strain is zero, a phenomenon known as "plastic deformation with no volume change." Stress deviation is the primary cause of inelastic deformation in materials; therefore, the main

factor driving plastic deformation in coal and rock masses is strain energy, not total strain energy. Consequently, studying stress deviation in rock masses is of great significance for investigating their elastic–plastic deformation and failure. In the following, the fourth strength theory will be utilized to evaluate the stability of the working face roof using strain energy as an indicator.

In rock mechanics, the total stress tensor σ_{ij} can be decomposed into the spherical stress tensor and the deviatoric stress tensor σ_{ij}:

$$\sigma_{ij} = \sigma_m \delta_{ij} + s_{ij} \quad (1)$$

Here, $\sigma_m = \frac{1}{3}(\sigma_1 + \sigma_2 + \sigma_3)$ represents the mean stress; δ_{ij} denotes the Kronecker delta; and s_{ij} denotes the partial stress tensor.

The second invariant J_2 of the partial stress tensor is a key physical quantity for measuring the degree of shear deformation in rock, and its expression is as follows:

$$J_2 = \frac{1}{2} s_{ij} s_{ij} = \frac{1}{6}\left[\left(\sigma_1 - \sigma_2\right)^2 + \left(\sigma_2 - \sigma_3\right)^2 + \left(\sigma_3 - \sigma_1\right)^2\right] \quad (2)$$

In this equation, σ_1, σ_2, and σ_3 represent the maximum principal stress, intermediate principal stress, and minimum principal stress, respectively.

Furthermore, the second invariant of the partial stress tensor is related to the strain energy of shape change (distortion energy) $\boldsymbol{W_F}$. The total strain energy density $\boldsymbol{W}$ of a rock mass under external loading consists of the volume change energy $\boldsymbol{W_v}$ and the distortion energy $\boldsymbol{W_F}$. According to the generalized Hooke's law, the distortion energy $\boldsymbol{W_F}$ depends solely on the deviatoric stress state, and its formula is derived as follows:

$$W_F = \frac{1+v}{3E} \cdot 3J_2 = \frac{1+v}{E} J_2 = \frac{J_2}{2G} \quad (3)$$

where E is the elastic modulus; v is the Poisson's ratio; and G is the modulus of rigidity or shear modulus.

From the above equation, it can be seen that when the modulus of rigidity G is fixed, there is a linear relationship between the second invariant of the deviatoric stress and the deformation energy.

4.2. Spatial Evolution Analysis of Strain Energy in the Working Surface of a Folded Structure

To obtain the energy variation characteristics of the folded structural zone and thereby analyze the stability of the working face roof, we will use the Fish language to monitor the deviatoric stresses in the mining area and generate strain energy distribution contour plots. We will then select contour plots at characteristic points where energy partitioning is distinct for analysis. Figure 10 shows contour plots of the strain energy distribution as the working face advances to various turning points.

As shown in Figure 10, under the influence of mining operations in the working face, the distribution of deformation energy in the fold structure zone exhibits distinct regional characteristics. Strain energy is concentrated in the rock mass surrounding the goaf, the drift, and the axial zone of the anticline; in particular, deformation energy reaches a peak (which is a local maximum) at the intersection of these three areas. This makes the roof prone to instability and failure under the action of deviated stress. This area is therefore a key zone for prevention and control, whereas the region near the synclinal axis is in a low-energy zone, where the roof is relatively stable.

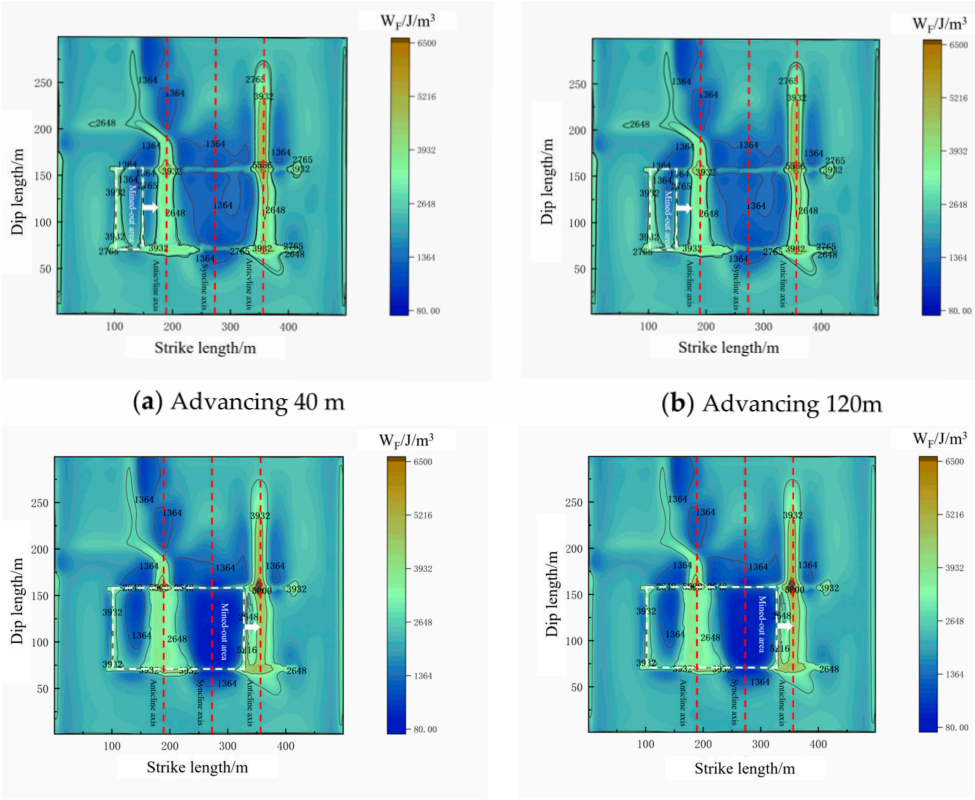

Figure 10. Aberration energy distribution cloud for different propulsion distances.

From the perspective of an advanced position, although significant advanced abutment stress exists at each turning point, there are significant differences in the distribution of strain energy. First, during the initial 60 m advance to the first turning point, strain energy values are high at the coal face and the cut-off point, with the cut-off point serving as the energy peak of the mining area; As advancement continued through the synclinal axis to the second inflection point, the strain energy at the cut-off point decreased, and the synclinal axis became the peak energy point of the mining area. At this stage, the stress concentration was concentrated at the haulage gate, where the strain energy of the roadhead reached 5446 J/m^3, making it prone to roof falls that could induce roof failure in the goaf. However, the energy at the coal face was lower, and the roof was more stable. In the second stage, when the advance reaches 220 m, the system is at the third inflection point. Similar to the first stage, the working face is in the upward mining phase. A large amount of strain energy accumulates in the roof ahead of the working face, and together with the energy at the synclinal axis, it forms a bimodal energy field. At this point, if the energy threshold is reached, the mining area will experience a large-scale roof collapse, affecting the safe production of the working face. When the working face advances to 280 m, it reaches the fourth inflection point. After the working face passes the axis of the anticline, the strain energy from the bimodal energy field transfers to the two side drifts. Compared to the previous inflection point, the strain energy in the roof of the haulage gate increases from 5891 J/m^3 to 7183 J/m^3, a rise of 21.9%; the strain energy in the return air drift roof increased from 5189 J/m^3 to 6024 J/m^3, a 16.1% increase. Furthermore, the strain energy continues to rise as the distance between the two drifts and the working face increases. Under deviatoric stress, the drift roofs undergo plastic deformation until roof collapse.

Field measurements have revealed that roof stability is poorest at the inflection points of anticlines and synclines, where large-scale collapses are likely to occur. This finding is fully consistent with the theoretical patterns derived from numerical simulations, demon-

strating that the model is highly reliable and can serve as a theoretical basis for subsequent research into rock mass control and the prevention of roof-related hazards.

5. Conclusions

This paper examines the engineering geological conditions of a high-seam mining face in Coal Seam No. 2 at a certain mine. Using Rhino+Hypermesh modeling technology, a three-dimensional numerical model was constructed to analyze the stress distribution in the surrounding rock and the evolution of energy during mining operations in a folded structural zone. The main conclusions are as follows:

(1) When the face advances upward in a reverse-dipping direction toward the anticline crest, the advance abutment stress reaches a minimum value of 4.84 MPa at the crest. In the goaf, the stress in the waste rock reaches a maximum of 1.53 MPa at the inflection point. During the downward dip mining process of the working face, the bearing stress exhibits an increasing trend; when advancing to the synclinal trough point, the bearing stress drops to its minimum value, and at the inflection point of the dip mining in the stress concentration zone, the bearing stress reaches a maximum of 7.6 MPa.

(2) From the perspective of the working face surrounding rock, during the initial anticline upward mining phase, the bearing stress is higher on the side of the haulage gate with greater curvature, reaching a maximum of 6.88 MPa, and drops sharply when advancing near the ridge point; during the synclinal down-dip and up-dip mining phases, the bearing stress is higher at the working face with smaller curvature and reaches a trough at the trough point; during the anticline down-dip mining phase, the fold curvature is smaller, and the bearing stress peaks at the inflection point, beginning to decrease after passing the turning point.

(3) At the start of mining in a folded strata face, the strain energy at the cut-off point is at its peak. As the face advances to the second inflection point, the strain energy at the cut-off point decreases, and the axis of the anticline becomes the energy peak point of the mining area. At this point, the deviatoric stress is concentrated at the location of the haulage gate at the ridge point, and the strain energy of the roadhead reaches 5446 J/m^3; as mining advances to the third inflection point, a large amount of strain energy accumulates in the roof ahead of the working face, forming a bimodal energy field in conjunction with the ridge point. By the fourth inflection point, the strain energy in the headings on both sides of the goaf increases with the distance from the lagging working face, rising by 21.9% (transport heading) and 16.1% (return air heading).

Author Contributions: Conceptualization, F.X.; Supervision, F.X.; Methodology, F.X. and Z.Q.; Funding acquisition, F.X.; Writing—review and editing, F.X. and P.W.; Writing—original draft, Z.Q.; Validation, Z.Q.; Visualization, Z.Q., P.W. and Q.H.; Investigation, P.W.; Data curation, Q.H.; Formal analysis, Q.H. All authors have read and agreed to the published version of the manuscript.

Funding: This research was funded by the National Natural Science Foundation (52574112).

Institutional Review Board Statement: Not applicable.

Informed Consent Statement: Not applicable.

Data Availability Statement: The original contributions presented in this study are included in the article. Further inquiries can be directed to the corresponding author.

Conflicts of Interest: Author Pan Wu was employed by Guoneng Shendong Coal Group Co., Ltd. The remaining authors declare that the research was conducted in the absence of any commercial or financial relationships that could be construed as a potential conflict of interest.

References

1. Liu, Y.Q. Research and Trend Analysis of the Global Coal Market in 2023–2024. *China Coal* **2024**, *50*, 164–169.
2. Foster, D.A.; Gray, D.R. Evolution and structure of the Lachlan fold belt (Orogen) of Eastern Australia. *Annu Rev. Earth Planet Sci.* **2000**, *28*, 47–80. [CrossRef]
3. Dou, L.M.; Tian, X.Y.; Cao, A.Y.; Gong, S.; He, H.; He, J.; Cai, W.; Li, X. Current Status and Challenges in the Prevention and Control of Coal Mine Rockburst in China. *J. Coal Sci. Eng.* **2022**, *47*, 152–171.
4. Wang, L.H.; Cao, A.Y.; Guo, W.H.; Dou, L.M.; Wen, Y.Y.; Xue, C.C.; Hu, Y.; Lv, D.Z. Mechanism and Instability Patterns of Roadway Rockburst in "Fault-Fold" Tectonic Zones. *J. Min. Saf. Eng.* **2023**, *40*, 69–81+90.
5. Cao, D.Y.; Zhan, W.F.; Li, H.T.; Li, X.; Wei, Y. Tectonic Background and Risk Zone Delineation of Dynamic Geological Hazards in Chinese Coal Mines. *J. Coal Sci. Eng.* **2020**, *45*, 2376–2388.
6. Zhang, K.; Wang, L.; Cheng, Y.; Li, W.; Kan, J.; Tu, Q.; Jiang, J. Geological control of fold structure on gas occurrence and its implication for coalbed gas outburst: Case study in the Qinan coal mine, Huaibei coalfield, China. *Nat. Resour. Res.* **2020**, *29*, 1375–1395. [CrossRef]
7. Yang, Z.Q.; Liu, C.; Liu, S.J.; Pei, Z.Y.; Shu, T. Mechanism of Rockburst Induced by Changes in Coal Seam Dip Angle in the Wing Area of a Fold and Its Prevention and Control. *Min. Saf. Environ. Prot.* **2024**, *51*, 82–89.
8. Lou, J.; Gao, F.; Yang, J.; Ren, Y.; Li, J.; Wang, X.; Yang, L. Characteristics of evolution of mining-induced stress field in the longwall panel: Insights from physical modeling. *Int. J. Coal Sci. Technol.* **2021**, *8*, 938–955. [CrossRef]
9. Xiao, F.K.; Mo, R.H. Study on Creep Energy Dissipation and Damage Deformation Characteristics of Rock Under Unloading Confining Pressure. *Rock Mech. Rock Eng.* **2025**, 1–16. [CrossRef]
10. Ju, X. A Study on Rock Mass Stress in High-Stress Highway Tunnels Within Compressive Fold Structures. Master's Thesis, Lanzhou University of Technology, Lanzhou, China, 2022.
11. Xu, J.S.; Pan, P.Z.; Chen, J.Q.; Zhao, S.K.; Wu, Z.H. A Study on the Evaluation of Rockburst Hazards in Coal Seams in Folded Areas Based on In-situ Stress Inversion. *Coal Sci. Technol.* **2023**, *51*, 35–45.
12. Wang, S.B.; Zhang, X. The Relationship Between Geological Structures and Geological Stresses in Underground Coal Mines. *J. Coal Sci. Eng.* **2008**, 738–742. [CrossRef]
13. Cheng, X.; Qiao, W.; Dou, L.; He, H.; Ju, W.; Zhang, J.; Song, S.; Cui, H.; Fang, H. In-situ stress field inversion and its impact on mining-induced seismicity. *Geomat. Nat. Hazards Risk* **2023**, *14*, 176–195. [CrossRef]
14. Xue, C.; Cao, A.; Lv, G.; Wen, Y.; Liu, Y.; Wang, S.; Hao, Q. Study on stress evolution law and rock burst mechanism in upright fold structure area of deep mine. *Geomat. Nat. Hazards Risk* **2023**, *14*, 2218013. [CrossRef]
15. Kang, H.P.; Wang, J.H.; Gao, F.Q. Characteristics of Stress Distribution in Surrounding Rock of Tunneling working faces and Their Relationship with Support. *J. Coal Sci. Eng.* **2009**, *34*, 1585–1593.
16. Kang, H.P.; Wu, Z.G.; Gao, F.Q.; Ju, W.J. Influence of Underground Geological Structures on Soil Stress Distribution in Coal Mines. *J. Rock Mech. Eng.* **2012**, *31*, 2674–2680.
17. Tang, L.; Tu, S.H.; Tu, H.S.; Zhang, L.; Li, W.L. Evolutionary Patterns and Control Techniques of Mining-Induced Stresses in Surrounding Rock in Folded Structural Zones. *J. Min. Saf. Eng.* **2025**, *42*, 636–647.
18. Rong, H.; Li, N.; Cao, C.; Wang, Y.; Wei, S.; Li, J.; Li, M. A method for assessing the risk of rockburst based on coal-rock mechanical properties and In-Situ ground stress. *Sci. Rep.* **2024**, *14*, 26073. [CrossRef]
19. Guo, W.; Cao, A.; Hu, Y.; Xue, C.; Liu, Y.; Lv, D. Stress distribution and rockburst characteristics of roadway group under the influence of fault and fold structures: A case study. *Geomat. Nat. Hazards Risk* **2022**, *13*, 736–761. [CrossRef]
20. Bai, J.; Dou, L.; Li, J.; Zhou, K.; Cao, J.; Kan, J. Mechanism of coal burst triggered by mining-induced fault slip under high-stress conditions: A case study. *Front. Earth Sci.* **2022**, *10*, 884974. [CrossRef]
21. Cao, A.; Xue, C.; Wu, Y.; Wang, S.; Guo, W. Study on mechanism of rock burst in fold structure area of coal mine and its prevention practice. *Coal Sci. Technol.* **2021**, *49*, 82–87.
22. Lu, C.; Zhang, X.; Xiao, Z.; Wang, C.; Wang, B.; Zhou, T.; Li, H.; He, Z. Study on controlling law of fold structure on evolution of mining stress in deep mines. *Coal Sci. Technol.* **2023**, *48*, 44–50. [CrossRef]
23. Wang, G.; Gong, S.; Dou, L.; Wang, H.; Cai, W.; Cao, A. Rockburst characteristics in syncline regions and microseismic precursors based on energy density clouds. *Tunn. Undergr. Space Technol.* **2018**, *81*, 83–93. [CrossRef]
24. Zhou, Y.; Lin, G.; Gong, F.X.; Liu, S.L.; Zhang, D.S. Variations in Maximum Principal Stress and Horizontal Strain During Single-Layer Folding Deformation and Their Influencing Factors. *Tecton. Ore Depos.* **2007**, *31*, 37–43.
25. Wang, J.; Li, G.; Wang, W.; Liu, H.; Wang, R.; Zhang, H.; Yuan, S. Distribution Characteristics of Mining-Induced Stress Fields and Surrounding Rock Control Technology in Adjacent Working Faces Within Fold Structure Zones. *Processes* **2025**, *13*, 1534. [CrossRef]
26. Liu, C.; Zhang, Y.; Song, J.; Xu, R.C. Stress Evolution in the Surrounding Rock of Adjacent Drifts in Folded Structural Zones and Techniques for Preventing Rockburst. *Coal Mine Saf.* **2023**, *54*, 100–106.

27. Jing, L. A review of techniques, advances and outstanding issues in numerical modelling for rock mechanics and rock engineering. *Int. J. Rock Mech. Min.* **2003**, *40*, 283–353. [CrossRef]
28. Hamdi, P.; Ufrecht, S.; Achtziger-Zupančič, P.; Bröker, K.; Ma, X.; Amann, F. Understanding the Regional Stress in Active Tectonic Regime Using 3D Numerical Modeling, Case Study of BedrettoLab, Switzerland. *Rock Mech. Rock Eng.* **2025**, *58*, 12187–12206. [CrossRef]
29. Zhang, B.; Zhao, H.; Yang, G.; Wang, X.; Gao, L.; Ji, D. Spatiotemporal evolution of deep fault slip and its coupled dynamic loading influence zone. *Soil Dyn. Earthq. Eng.* **2026**, *203*, 110021. [CrossRef]
30. Wang, H.; Deng, D.; Jiang, C.; Shi, R.; Yan, X. Study on evolution characteristics of uneven stress field in mining-induced fold tectonic area. *Coal Sci. Technol.* **2020**, *48*, 59–69. [CrossRef]
31. Chen, G.; Dou, L.; Wang, Z. The study on prevention of rockburst when mining in folding structure areas. In *Proceedings of the 2011 Asia-Pacific Power and Energy Engineering Conference*; IEEE: Wuhan, China, 25–28 March 2011.
32. Yu, Y.; Ma, L.; Zhang, D.; Su, F.; Wang, G. Approach for numerical modeling of strain-hardening materials using double-yield model. *Rock Mech. Rock Eng.* **2022**, *55*, 7357–7367. [CrossRef]